ACS APPLIED MATERIALS & INTERFACES

www.acsami.org

Research Article

Printed Ultrastable Bioplasmonic Microarrays for Point-of-Need Biosensing

Heng Guo, Ze Yin, Myeong Namkoong, Yixuan Li, Tan Nguyen, Elizabeth Salcedo, Ivanna Arizpe, and Limei Tian*

Cite This: *ACS Appl. Mater. Interfaces* 2022, 14, 10729–10737

Read Online

ACCESS | Metrics & More | Article Recommendations | Supporting Information

ABSTRACT: Paper-based point-of-need (PON) biosensors are attractive for various applications, including food safety, agriculture, disease diagnosis, and drug screening, owing to their low cost and ease of use. However, existing paper-based biosensors mainly rely on biolabels, colorimetric reagents, and biorecognition elements and exhibit limited stability under harsh environments. Here, we report a label-free paper-based biosensor composed of bioplasmonic microarrays for sensitive detection and quantification of protein targets in small volumes of biofluids. Bioplasmonic microarrays were printed using an ultrastable bioplasmonic ink, rendering the PON sensors excellent thermal, chemical, and biological stability for their reliable performance in resource-limited settings. We fabricated silicone hydrophobic barriers and bioplasmonic microarrays with direct writing and droplet jetting approaches on a three-dimensional (3D) nanoporous paper. Direct writing hydrophobic barriers can define hydrophilic channels less than 100 μm wide. High-resolution patterning of hydrophilic test domains enables the handling and analysis of small fluid volumes. We show that the plasmonic sensors based on a vertical flow assay provide similar sensitivity and low limit of detection with a 60 μL sample volume compared to those with 500 μL samples based on an immersion approach and can shorten assay time from 90 to 20 min.

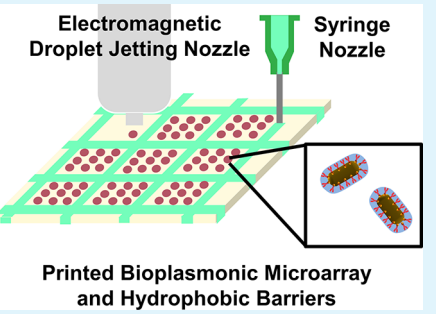

KEYWORDS: *localized surface plasmon resonance, plasmonic biosensor, plasmonic microarray, bioprinting, direct ink writing, silicone hydrophobic barrier, vertical flow assay*

INTRODUCTION

Point-of-need (PON) diagnostics demand low-cost, sensitive, specific, and stable biosensors that enable rapid, user-friendly operation under resource-limited settings.[1−3] Lateral and vertical flow assays based on low cost materials such as paper and colorimetric readout are attractive for various applications, including food safety, agriculture, disease diagnosis, and drug screening.[4−9] However, most of these assays rely on labeling and exhibit limited stability under harsh environments. Plasmonic biosensors based on localized surface plasmon resonance (LSPR) can provide label-free, highly sensitive quantification of biomarkers in complex biofluids.[10−17] Recent advances in preserving the functionality of plasmonic biosensors have improved the stability of these biosensors and their reliable performance for PON diagnostics.[18−21] For example, metal-organic framework coating can retain the biorecognition capability of antibodies immobilized on the nanostructure surface in plasmonic biosensors after exposure to elevated temperatures.[19,20] However, this approach requires protective coating removal before introducing the sample to the sensors. Alternatively, organosiloxane polymer-encapsulated antibodies render plasmonic biosensors improved thermal, mechanical, chemical, and biological stability.[18,22] However, these sensors rely on rigid two-dimensional (2D) substrates and cannot handle small-volume biofluids for biomarker quantification. A plasmonic biosensing platform with stable sensing components and the capability of handling small-volume biofluids is needed for reliable and user-friendly diagnostics at the PON.

A simple, cost-effective, and scalable fabrication is essential for the broad application of PON biosensors. Current low-cost fabrication methods of paper-based microfluidic devices mainly rely on wax printing to yield hydrophobic barriers.[23−25] However, wax printing has several limitations, including low resolution, high-temperature process, and storage limitation. The smallest functional hydrophilic channel width defined by hydrophobic wax barriers is ∼0.5 mm.[26] The penetration of wax through porous substrates relies on heating with the reported working temperature in the range of 90−175 °C.[27,28] The high-temperature processing is not compatible with temperature-sensitive materials, including bioreagents and

Received: December 17, 2021
Accepted: February 4, 2022
Published: February 16, 2022

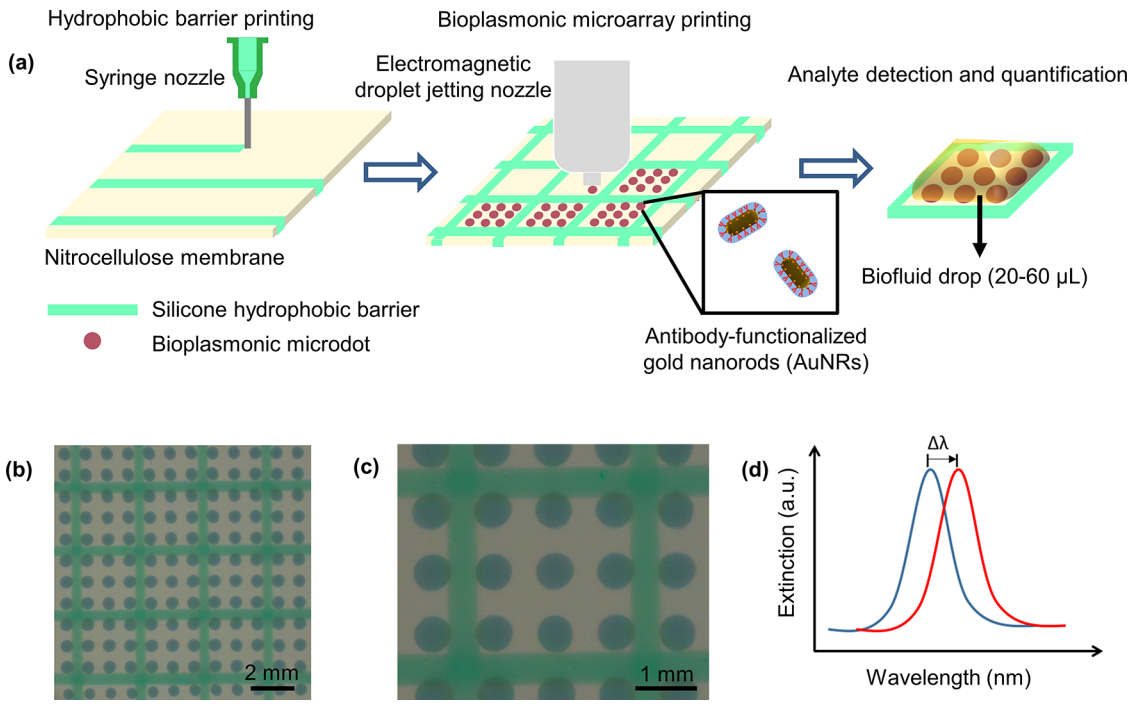

Figure 1. Printed plasmonic biosensors. (a) Schematic illustration of the hydrophobic barrier and bioplasmonic microarray printing to fabricate plasmonic biosensors for small-volume sample analysis. (b, c) Optical microscope images of printed biosensors with a unit dimension of 3 mm × 3 mm. Each unit comprises printed silicone hydrophobic barriers (light green) and bioplasmonic microdots. (d) Illustration of the sensing mechanism based on the LSPR wavelength shift of plasmonic nanostructures.

nitrocellulose papers. In addition, the melting of the wax during long-term storage can cause sample contamination and changes in hydrophilic channel dimensions.[23] Alternatively, diluted poly(dimethylsiloxane) (PDMS) prepolymer was used to pattern hydrophobic barriers involving toxic solvents, such as hexane and toluene.[29−31] Silicone hydrophobic barriers are more compatible with some organic solvents than wax hydrophobic barriers. Those solvents include methanol and acetonitrile, which are commonly used in liquid chromatography and nonaqueous capillary electrophoresis.[30,32,33] To realize small-volume sample handling and analysis, PDMS hydrophobic barriers can be fabricated on porous substrates by inkjet printing, providing a hydrophilic channel width of 60 μm.[31] However, contamination across multiple inks contained by the cartridges and print heads often occurs. Furthermore, the fabrication of plasmonic biosensors on a microfluidic platform typically involves tedious and expensive processes, including lithography, etching, assembly of LSPR nanotransducers and microfluidic chips, and surface functionalization.[34−36] An efficient fabrication strategy is still needed to realize an integrated plasmonic-microfluidic sensing platform.

This work reports plasmonic biosensors printed on three-dimensional (3D) porous papers composed of bioplasmonic microarray and silicone hydrophobic barriers. Silicone hydrophobic barriers were patterned by continuously extruding silicone prepolymer solution with well-controlled flow rates. The width of hydrophilic channels can reach less than 100 μm, allowing for small-volume fluid handling. The bioplasmonic microarrays were fabricated by droplet printing of ultrastable bioplasmonic ink. The printed plasmonic biosensors based on a vertical flow assay can simultaneously analyze multiple samples of 20−60 μL without compromising the sensitivity of biosensors. We demonstrate that ultrastable plasmonic sensors with encapsulated antibodies exhibit excellent thermal, chemical, and biological stability, suitable for PON applications.

RESULTS AND DISCUSSION

Printed plasmonic biosensors comprise hydrophobic barriers and plasmonic microarrays patterned on a 3D porous substrate (Figure 1a). The hydrophobic barriers confine biofluids to interact with the antibodies on the plasmonic nanostructure surface. The dimension of a hydrophilic domain confined by hydrophobic barriers is designed based on the biofluid volume of interest. For example, the hydrophobic square with a width of 2 mm can confine the volume of biofluids up to ∼6 μL. The hydrophobic barriers are realized by direct extruding a silicone prepolymer solution with a syringe nozzle and well-controlled flow rates. Plasmonic microarrays are patterned by printing encapsulated antibody-functionalized gold nanorods (AuNRs) using an electromagnetic droplet jetting nozzle. Previously, we showed that the organosiloxane encapsulation of antibodies significantly improved the thermal, chemical, and biological stability of plasmonic biosensors on 2D rigid surfaces.[18] Here, we print the ultrastable bioplasmonic array along with hydrophobic barriers on a 3D substrate, nitrocellulose (NC) paper, to quantify proteins in a small volume of biofluids. NC paper is a commonly used substrate in lateral and vertical flow assays due to its high affinity to biomolecules, large surface area, and wicking properties. Figure 1b,c shows optical microscope images of the printed plasmonic arrays confined within silicone hydrophobic barriers. For easy visualization, a green dye was added to the silicone precursor solution. The printed hydrophobic barriers have a uniform width of ∼500 μm in horizontal and vertical directions. The center distance between hydrophobic barriers is 3 mm, defining a hydrophilic domain of 2.8 mm × 2.8 mm. Each hydrophilic domain contains 3 × 3 plasmonic microdots with a diameter of ∼600

https://doi.org/10.1021/acsami.1c24458
ACS Appl. Mater. Interfaces 2022, 14, 10729−10737

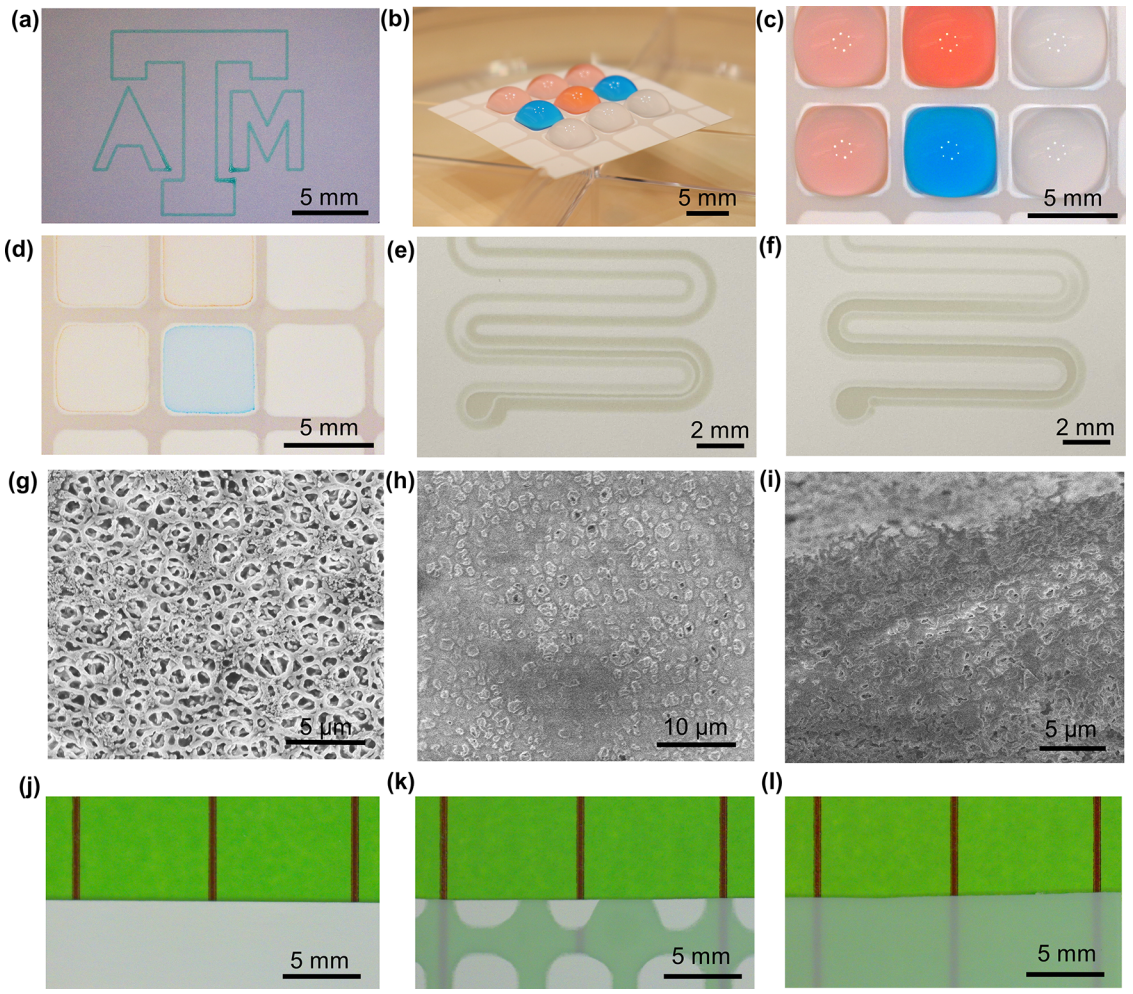

Figure 2. Hydrophobic barrier characterization. (a) Optical microscope image of Texas A&M Logo printed with silicone prepolymers on an NC paper. Optical images of droplets with four colors confined within hydrophilic domains before (b, c) and after (d) drying. (e, f) Optical images of liquid propagating along a microchannel with varying widths. (g) Scanning electron microscope (SEM) image of a pristine NC paper. SEM images of (h) the top view and (i) the cross section of NC papers with printed silicone hydrophobic barriers. Optical microscope images of NC papers (j) without silicone, (k) with printed silicone barriers, and (l) with a silicone coating placed above a green background.

μm. The LSPR wavelength change measured from plasmonic microdots before and after the targets bind to the antibodies on the AuNR surface can quantify the concentration of protein targets (Figure 1d).

We first characterized the hydrophobic barrier printed with the silicone prepolymer solutions of different viscosities. The solution with lower viscosity is expected to wet the NC surface and propagate inside a porous matrix more efficiently. We chose silicone prepolymer solutions with a viscosity of 3000 cps (Ecoflex 00-30) and 150 cps (Rubber Glass) to compare the performance of corresponding printed hydrophobic barriers. The silicone prepolymer solutions do not need toxic organic solvents to adjust viscosity. The hydrophobic barrier was printed by continuously extruding a silicone ink, i.e., the silicone prepolymer solution, with an ink extrusion rate of 0.08–0.16 μL/s and a printing speed of 1 mm/s. This approach is more efficient than inkjet printing (droplet printing), which often suffers from contamination across inks and nozzle blockage. Figure 2a shows a printed Texas A&M logo with a silicone solution on a nitrocellulose paper with a 0.45 μm pore size. It takes 3 times printing to define a hydrophobic barrier using Ecoflex, which completely blocks the liquid from spreading (Figure S1). In comparison, the hydrophobic barrier can be achieved by one-time printing of a low-viscosity silicone ink (Rubber Glass) with an ink extrusion rate of 0.08 μL/s due to its easy penetration through the pores. The contact angles of water and 1× phosphate-buffered saline (PBS) on the cured Rubber Glass were measured to be ~106°, confirming its hydrophobic surface (Figure S2). Figure 2b,c shows 40 μL of droplets with four colors confined within hydrophilic domains with a dimension of ~6 mm × 6 mm. This hydrophobic barrier configuration printed with Rubber Glass was used in the sensing experiments described below. We applied an absorbance pad under the nitrocellulose paper to drive the liquid flow vertically, simulating the liquid transport in a vertical flow assay. We did not observe any dye diffusion or contamination across different domains before and after drying (Figure 2d).

The printing strategy to define hydrophobic barriers can be applied on nitrocellulose papers with other pore sizes. The design pattern and locally dispensed volume of silicone ink can control the dimension of hydrophilic channels. Figure 2e,f shows a lateral flow pattern with varying microfluidic channel widths on a nitrocellulose paper with a 10 μm pore size. By changing the dispense volume of the silicone ink, the realized channel width can be less than 100 μm (Figure 2e). This

https://doi.org/10.1021/acsami.1c24458
ACS Appl. Mater. Interfaces 2022, 14, 10729−10737

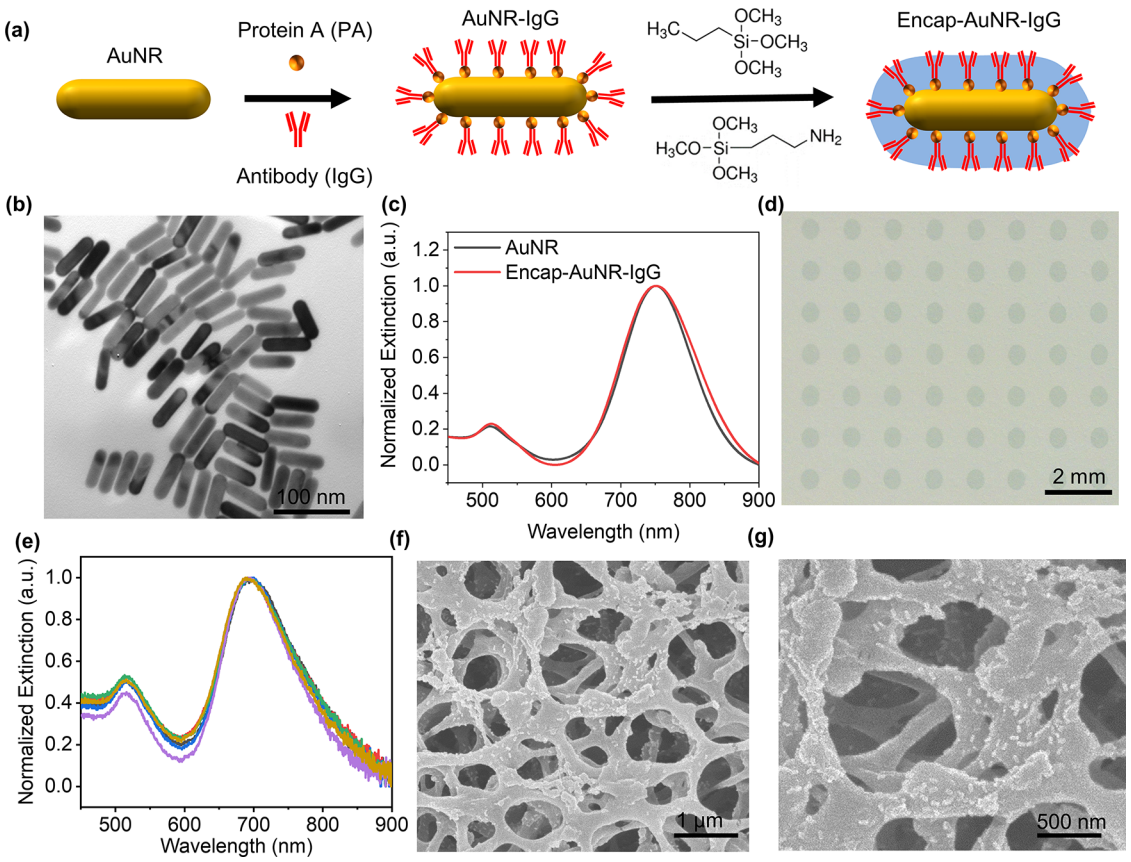

Figure 3. Printed bioplasmonic microarray characterization. (a) Schematic illustration showing the functionalization and encapsulation of AuNRs in a solution. (b) TEM image of AuNRs. (c) Normalized extinction spectra of AuNRs before and after functionalization and encapsulation. (d) Optical microscope image of printed bioplasmonic array. (e) Six spectra collected from different plasmonic microdots. (f, g) SEM images of plasmonic nanostructures distributed on the NC paper.

fabrication capability allows microfluidic devices to handle a small volume of biofluids for running lateral and vertical flow assays. Scanning electron microscope (SEM) images characterize the changes in structure and morphology of NC papers before and after silicone prepolymers penetrate the porous paper and fill the pores. Figure 2g reveals the porous morphology of a 0.45 μm NC paper. The silicone prepolymer solution with a low viscosity fills all of the pores in the paper, confirmed by the top view and cross-sectional SEM images collected after silicone curing (Figure 2h,i). Similar morphology changes were observed with 10 μm NC papers (Figure S3). The NC paper with silicone fillers changes the optical properties from opaque to translucent (Figure 2j–l). The optical transmittance of the hydrophobic region in the NC paper is measured to be around 42% in the visible wavelengths of 400–700 nm (Figure S4). This feature is helpful to assemble and align different functional layers in a vertical flow assay.

The bioplasmonic ink was prepared following our previous protocol (Figure 3a).[18] AuNRs were first functionalized with protein A and then human immunoglobulin G (IgG) antibodies in the solution. Human IgG and antihuman IgG (anti-H IgG) were used as a model pair of antibodies and protein targets in the following experiments. After functionalization, an organosiloxane polymer layer was coated on AuNR-IgG bionanoconjugates through in situ polymerization of trimethoxypropylsilane (TMPS) and (3-aminopropyl)-trimethoxysilane (APTMS) in borate-buffered saline. The organosiloxane polymer protects IgG antibodies from degradation under harsh conditions.[18,22] The polymer-encapsulated AuNR-IgG bionanoconjugates solution is described as bioplasmonic ink. AuNRs were used as nanotransducers because of the high refractive index sensitivity and a tunable longitudinal LSPR wavelength (LLSPR) by changing the aspect ratio.[37] The shift in the LLSPR wavelength was used to quantify the binding of molecules on the AuNR surface because of the higher refractive index sensitivity of the longitudinal LSPR band than that of the transverse band of AuNRs.[37,38] Figure 3b shows a transmission electron microscopy (TEM) image of as-synthesized AuNRs with 53.4 ± 4.7 nm in length and 14.0 ± 1.9 nm in diameter. The average values and standard deviations were calculated from 100 AuNRs in TEM images. The extinction spectrum of AuNRs after encapsulation exhibits 5 nm red shift in the LLSPR wavelength, resulting from the increase in the refractive index near the AuNR surface (Figure 3c). The LLSPR wavelength shift was quantified by the second peak position of the Gaussian fitted extinction spectra (Figure S5). The full width at half-maximum intensity (FWHM) of the spectra shows little change, confirming that the bionanoconjugates are well dispersed in the solution without forming aggregations.

We printed the bioplasmonic ink on a 0.45 μm NC paper using an electromagnetic droplet jetting nozzle. The jetting pressure and microvalve open time can control the dot size. The nanoporous NC paper was chosen to provide efficient interaction between AuNR-IgG and protein targets while

https://doi.org/10.1021/acsami.1c24458
ACS Appl. Mater. Interfaces 2022, 14, 10729–10737

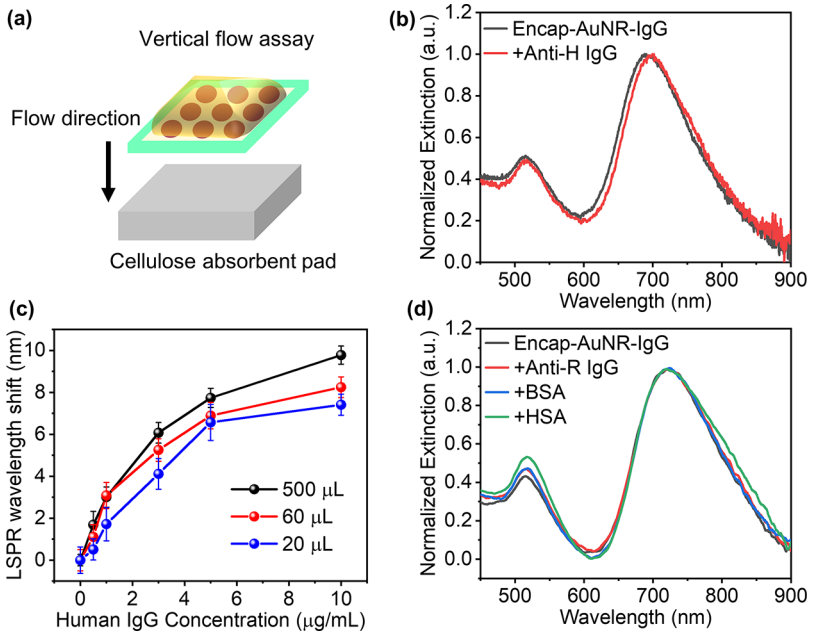

Figure 4. Sensitivity and selectivity of plasmonic biosensors. (a) Schematic illustration of a plasmonic biosensor based on a vertical flow assay. (b) Normalized extinction spectra of the plasmonic biosensor before and after exposure to 10 μg/mL anti-H IgG. (c) LLSPR wavelength shifts of plasmonic biosensors after exposure to 20, 60, and 500 μL of anti-H IgG solution at varying concentrations. Error bars represent standard deviations from three biosensors. (d) Normalized extinction spectra of plasmonic biosensors before and after exposure to 10 μg/mL antirabbit IgG, 10 mg/mL BSA, and 30 mg/mL HSA.

supporting fluid transport. Figure 3d shows a printed bioplasmonic microarray with a uniform dot size of 580 μm in diameter with a jetting pressure of 1 kPa and valve open time of 1 ms. The immobilization of bioplasmonic ink on the NC paper relies on the combination of weak interactions, including electrostatic and hydrophobic interactions. Figures 3e and S6 show extinction spectra collected from six different bioplasmonic microdots. The LLSPR wavelength of bionanoconjugates on the NC paper exhibits ~65 nm blue shift compared to that in the solution (Figure 3c,e). The standard deviation of LLSPR wavelength is less than 1 nm, setting the noise floor for quantifying protein targets. The small standard deviation results from the uniform distribution of bionanoconjugates on the NC paper, shown in SEM images (Figure 3f,g). The density of the bionanoconjugates depends on the concentration of the plasmonic ink, quantifiable with the extinction intensity. The bioplasmonic ink with an extinction intensity of 5 yields the bionanoconjugate density of ~80/μm^2 on the NC paper, quantified from the top surface in SEM images.

We assembled printed biosensors composed of bioplasmonic microarray and hydrophobic barriers on a cellulose absorbent pad to form a vertical flow assay (Figure 4a). The vertical flow assay can rapidly process biofluids and wash buffer.[39,40] In this assembly, biosensors comprise a 3 × 3 bioplasmonic microarray confined within a hydrophilic domain of 6 mm × 6 mm. We evaluated the sensitivity of plasmonic biosensors based on the vertical flow assay by analyzing 20 and 60 μL samples with varying concentrations of anti-H IgG. The vertical flow assay takes less than 20 min to complete the sample processing and 100 μL of 1× PBS washing to remove nonspecific bound proteins. For comparison, the sensitivity of plasmonic biosensors was measured after immersing them in 500 μL samples for 90 min. Figures 4b and S7 show the representative extinction spectra of bionanoconjugates before and after exposure to anti-H IgG of 10 μg/mL. The binding of anti-H IgG results in ~10 nm red shift in the LLSPR wavelength. The LLSPR wavelength shift increases with the increase in the concentration of anti-H IgG from 0.5 to 10 μg/mL (Figure 4c). The overall LLSPR shifts show a slight decrease with decreasing sample volumes. The lower limit of detection (LLOD) is ~0.5 μg/mL for 60 and 500 μL samples. In contrast, the LLOD increases to ~1 μg/mL for 20 μL samples. These results confirm that reducing the sample volume to 60 μL and shortening the assay time to ~20 min have a negligible effect on the LLOD of the target. We evaluated the selectivity of the plasmonic sensor by exposing the biosensor to high concentrations of interfering proteins, including 10 μg/mL antirabbit IgG, 10 mg/mL bovine serum albumin (BSA), and 30 mg/mL human serum albumin (HSA). Figures 4d and S8 show the extinction spectra of nanoconjugates before and after exposure to the interfering proteins. The LLSPR wavelength shifts are less than 1 nm, confirming negligible nonspecific binding. We also exposed the biosensors to the mixture of HSA and antihuman IgG and observed 20% decrease in the LLSPR wavelength shift compared to that exposed to only antihuman IgG (Figure S9). The reduced shift is likely due to minor contamination of the purchased human albumin with human IgG. The speculation is further confirmed by no decrease in the shift after exposing the biosensor to the mixture of BSA and antihuman IgG.

The biosensor stability is critical for their reliable performance under harsh environments in resource-limited settings. We examined the stability of printed biosensors with and without the molecular encapsulation of antibodies under harsh conditions, including elevated temperature, chemical, and biological denaturants. The biosensors composed of antibodies or other biomolecules are typically transported and stored under cold conditions to prevent degradation. Here, a high

https://doi.org/10.1021/acsami.1c24458
ACS Appl. Mater. Interfaces 2022, 14, 10729−10737

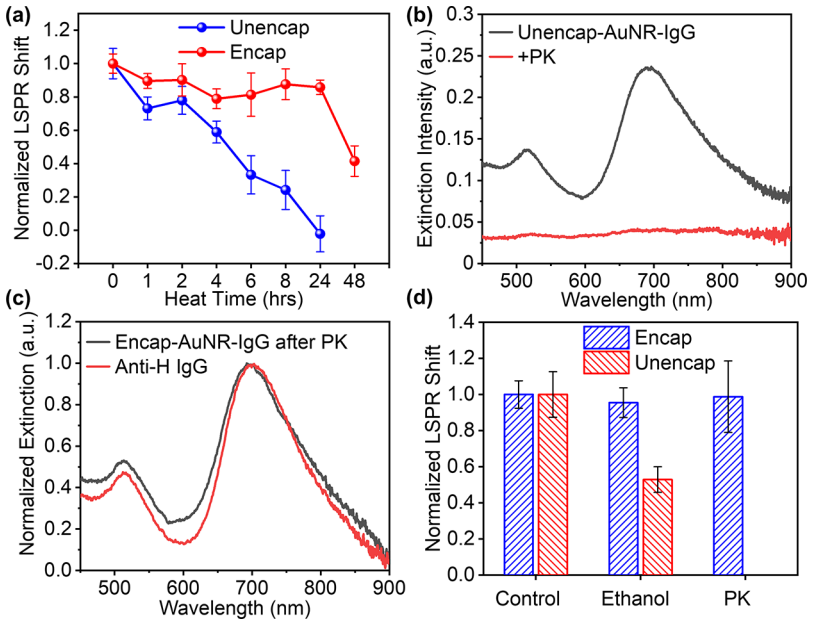

Figure 5. Stability of plasmonic biosensors. (a) Normalized LLSPR wavelength shifts of plasmonic biosensors with and without encapsulation after exposure to 60 °C for different durations and then 5 μg/mL antihuman IgG. Error bars represent standard deviations from three biosensors. (b) Extinction spectra of unencapsulated plasmonic biosensors before and after exposure to 100 μg/mL proteinase K. (c) Normalized extinction spectra of proteinase K-treated encapsulated biosensors before and after exposure to 5 μg/mL antihuman IgG. (d) Normalized LLSPR wavelength shifts of plasmonic biosensors with and without encapsulation after exposure to 75% ethanol and 100 μg/mL proteinase K and then 5 μg/mL antihuman IgG.

temperature of 60 °C is used to simulate extreme conditions during transport or storage. Furthermore, thermal-accelerated tests can speed up the degradation process. For thermal stability tests, the encapsulated and unencapsulated biosensors were kept under 60 °C for different durations and then exposed to anti-H IgG of 5 μg/mL (Figure 5a). The LLSPR wavelength shifts of the unencapsulated biosensors decrease with increasing the exposure duration to 60 °C. The unencapsulated biosensors show more than 50% decrease in the LLSPR wavelength shift following the anti-H IgG binding after thermal treatment for 6 h and no response to the anti-H IgG after 24 h under 60 °C, indicating a complete loss of biofunctionality. In contrast, the encapsulated biosensors show 14 and 59% decrease in the LLSPR wavelength shift following the anti-H IgG binding after 24 and 48 h under 60 °C, respectively.

We used proteinase K as a biological denaturant to evaluate the stability of encapsulated biosensors. We exposed plasmonic biosensors with and without antibody encapsulation to 100 μg/mL proteinase K solution for 15 min and then measured the LLSPR wavelength shifts after exposure to the anti-H IgG. For unencapsulated biosensors, extinction spectra collected after exposure to proteinase K do not exhibit distinguishable LSPR bands, caused by desorption of AuNR-IgG from the NC surface (Figure 5b). The desorption is likely induced by the altered interaction between the AuNR-IgG bionanoconjugates and the NC paper. In contrast, the extinction spectrum collected from the encapsulated biosensors after proteinase K exposure is well retained (Figure 5c). The LLSPR wavelength shift following the anti-H IgG binding remains similar to the shift from the biosensor without proteinase K treatment shown as the control in Figures 5d and S10. To test chemical stability, we exposed plasmonic biosensors with and without antibody encapsulation to 75% ethanol for 15 min and then measured the LLSPR wavelength shifts after exposure to the anti-H IgG. The LLSPR wavelength shift due to the anti-H IgG binding from encapsulated biosensors remains similar to the control, while the shift from unencapsulated biosensors decreases by ~50%. These results confirm the excellent stability of encapsulated plasmonic biosensors on NC papers, suitable for PON applications in resource-limited settings.

CONCLUSIONS

In this paper, we presented printed plasmonic biosensors composed of bioplasmonic microarrays and silicone hydrophobic barriers for rapid protein quantification in small-volume samples. The printed biosensors can simultaneously process multiple small-volume samples for target protein quantification. The plasmonic sensors show high sensitivity, selectivity, and thermal, chemical, and biological stability. Direct writing silicone prepolymer ink can yield hydrophobic barriers to define hydrophilic channels with a narrow width of ~100 μm. This approach is cost-effective, environmentally friendly, and time-efficient. The molecular encapsulation strategy and printing-based scalable fabrication can be easily extended to multiplexed biosensors for various protein biomarkers for disease diagnosis and health monitoring.

EXPERIMENTAL SECTION

Materials. Gold (III) chloride trihydrate ($HAuCl_4$, ≥99.9%), silver nitrate (≥99.0%), ascorbic acid (≥99.0%), sodium borohydride ($NaBH_4$, ≥98%), and cetyltrimethylammonium bromide (CTAB, ≥99%) were purchased from Sigma-Aldrich. Human IgG, goat antihuman IgG, mouse antirabbit IgG, protein A, borate-buffered saline, and phosphate-buffered saline (PBS, 10×) were purchased from Invitrogen. Bovine serum albumin (BSA) was purchased from Bio-world. Human serum albumin (HSA) was purchased from Gemini company. Trimethoxy(propyl)silane (TMPS, 95%), (3-aminopropyl)trimethoxysilane (APTMS, 99%), and proteinase K (recombinant) were purchased from Fisher Scientific. Nitrocellulose

https://doi.org/10.1021/acsami.1c24458
ACS Appl. Mater. Interfaces 2022, 14, 10729−10737

papers with 0.45 μm pore size were purchased from GE Healthcare. Nitrocellulose papers with 10 μm pore size were purchased from Sartorius. Rubber Glass and Ecoflex 00-30 were purchased from Smooth-On, Inc. Type 1 deionized (DI) water (18.2 mΩ·cm) was used in all experiments. All chemicals were used as received.

Gold Nanorod (AuNR) Synthesis. AuNRs were synthesized following a two-step seed-mediated growth method with modifications.[41,42] First, 9.75 mL of CTAB (0.1 M) and 0.25 mL of $HAuCl_4$ (10 mM) were mixed at room temperature. After 5 min, 0.6 mL of freshly prepared ice-cold $NaBH_4$ (10 mM) solution was introduced under vigorous stirring, and the mixture was stirred for another 10 min to form a seed solution. Second, a growth solution was prepared by mixing aqueous solutions of 38 mL of CTAB (0.1 M), 2 mL of $HAuCl_4$ (10 mM), 400 μL of $AgNO_3$ (10 mM), and 220 μL of ascorbic acid (0.1 M). Then, 48 μL of seed solution was added to the growth solution to initiate AuNR growth. The AuNR solution was kept overnight at room temperature. Finally, the AuNR solution was centrifuged once at 8000 rpm for 10 min and then redispersed in DI water for further use.

AuNR-H IgG Ink Preparation and Antibody Encapsulation. AuNRs were first functionalized with protein A by introducing 40 μL of protein A aqueous solution (100 μg/mL) into 2 mL of twice centrifuged AuNR solution. After overnight incubation at 4 °C, 70 μL of BSA solution (5 wt % in 1× PBS) was added into the AuNR-PA conjugate solution. The solution was centrifuged at 8000 rpm for 10 min to remove the excess protein A and then redispersed in 20 μL of borate-buffered saline. Subsequently, 80 μL of human IgG solution (100 μg/mL in 1× PBS) was added to the mixture and incubated for 45 min. For antibody encapsulation, 0.5 μL of TMPS and 0.5 μL of APTMS were added under gentle stirring. After 30 min, TMPS and APTMS of the identical amounts were added again. The mixture was then monitored with a UV−vis spectrophotometer, and the thickness of the encapsulation layer can be controlled by varying the incubation time. After that, 70 μL of BSA solution (5 wt % in 1× PBS) was introduced. The encapsulated AuNR-H IgG conjugates were centrifuged at 8000 rpm for 10 min to remove the excess TMPS and APTMS and then redispersed in 100 μL of borate-buffered saline.

Biosensor Printing and Measurements. For hydrophobic barrier printing, Ecoflex 00-30 part A and part B, or Rubber Glass part A and part B, were mixed, degassed, and then printed on a nitrocellulose paper via a 34 gauge blunt nozzle. The bioplasmonic ink was printed using an electromagnetic droplet jetting nozzle under the jetting pressure of 1 kPa. After printing, the nitrocellulose papers were immersed in the BSA solution (5 wt % in 1× PBS) overnight and then rinsed with 1× PBS and exposed to Tween-20 (1 wt % in 1× PBS) for 30 min and then air-dried. Subsequently, plasmonic biosensors composed of printed bioplasmonic microarray with hydrophobic barriers were tested, including sensitivity, selectivity, and stability. The biosensors were exposed to 20−500 μL of anti-H IgG solution with varying concentrations from 0.5 to 10 μg/mL to obtain calibration curves. The vertical flow assay takes less than 20 min to complete sample incubation and 1× PBS washing to remove nonspecific bound proteins. Extinction spectra were collected after the biosensors were left dried at room temperature for 1 h to ensure consistent results. To test the selectivity, the biosensors were exposed to interfering proteins, including BSA, HSA, and antirabbit IgG. For stability evaluation, the biosensors were first exposed to harsh conditions, including 60 °C up to 48 h, proteinase, and 75% ethanol. Then, LLSPR wavelength shifts were measured after anti-H IgG binding and compared to those from encapsulated biosensors with exposure to the same harsh conditions. The tests under each condition were conducted on more than three biosensors to account for sample-to-sample variation.

Characterization. A UV−vis spectrophotometer (Shimadzu UV-1900) was used to collect UV−vis extinction spectra of AuNR solution and monitor the AuNR surface functionalization. Transmission electron microscopy (TEM) images were collected using a high-resolution analytical TEM (JEOL JEM-2010). Scanning electron microscopy (SEM) images were collected using an ultra-high-resolution field emission SEM (JEOL JSM-7500F). A microspectrophotometer (CRAIC 308 PV) coupled to an optical microscope (Leica DM4M) was used to collect extinction spectra from NC papers with 20× objective in the range of 450−900 nm with 0.2 s exposure time in reflection mode.

■ ASSOCIATED CONTENT

Supporting Information

The Supporting Information is available free of charge at https://pubs.acs.org/doi/10.1021/acsami.1c24458.

Figure S1: Optical images of printed Ecoflex 00-30 hydrophobic barriers; Figure S2: Optical microscope images of aqueous droplets on the surface of Rubber Glass; Figure S3: SEM images of 10 μm NC paper with and without silicone; Figure S4: Optical transmittance of the hydrophobic region of the NC paper; Figure S5: Representative fitted extinction spectrum for the determination of the LSPR peak position; Figures S6−S8, S10: Magnified spectra in Figures 3e,4b,d, and 5c; and Figure S9: Normalized LLSPR wavelength shifts of plasmonic biosensors after exposure to antihuman IgG, HSA, mixture of HSA and antihuman IgG, and mixture of BSA and antihuman IgG (PDF)

■ AUTHOR INFORMATION

Corresponding Author

Limei Tian − *Department of Biomedical Engineering, and Center for Remote Health Technologies and Systems, Texas A&M University, College Station, Texas 77843, United States*; orcid.org/0000-0002-1931-8567; Email: ltian@tamu.edu

Authors

Heng Guo − *Department of Biomedical Engineering, Texas A&M University, College Station, Texas 77843, United States*

Ze Yin − *Department of Biomedical Engineering, Texas A&M University, College Station, Texas 77843, United States*

Myeong Namkoong − *Department of Biomedical Engineering, Texas A&M University, College Station, Texas 77843, United States*

Yixuan Li − *Department of Biomedical Engineering, Texas A&M University, College Station, Texas 77843, United States*

Tan Nguyen − *Department of Biomedical Engineering, Texas A&M University, College Station, Texas 77843, United States*

Elizabeth Salcedo − *Department of Biomedical Engineering, Texas A&M University, College Station, Texas 77843, United States*

Ivanna Arizpe − *Department of Biomedical Engineering, Texas A&M University, College Station, Texas 77843, United States*

Complete contact information is available at: https://pubs.acs.org/10.1021/acsami.1c24458

Notes

The authors declare no competing financial interest.

■ ACKNOWLEDGMENTS

The authors acknowledge the funding from the Department of Biomedical Engineering at Texas A&M University, the Texas A&M Engineering Experiment Station, the National Science

Foundation (Grant no. 1648451), and the National Institutes of Health (Grant no. 1R21EB029064-01A1). In addition, the use of instruments in the Texas A&M Materials Characterization Facility and Microscopy & Imaging Center is acknowledged.

REFERENCES

(1) Gubala, V.; Harris, L. F.; Ricco, A. J.; Tan, M. X.; Williams, D. E. Point of care diagnostics: status and future. *Anal. Chem.* **2012**, *84*, 487−515.
(2) Hu, J.; Wang, S.; Wang, L.; Li, F.; Pingguan-Murphy, B.; Lu, T. J.; Xu, F. Advances in paper-based point-of-care diagnostics. *Biosens. Bioelectron.* **2014**, *54*, 585−597.
(3) Nayak, S.; Blumenfeld, N. R.; Laksanasopin, T.; Sia, S. K. Point-of-Care Diagnostics: Recent Developments in a Connected Age. *Anal. Chem.* **2017**, *89*, 102−123.
(4) Joung, H.-A.; Ballard, Z. S.; Ma, A.; Tseng, D. K.; Teshome, H.; Burakowski, S.; Garner, O. B.; Di Carlo, D.; Ozcan, A. Paper-based multiplexed vertical flow assay for point-of-care testing. *Lab Chip* **2019**, *19*, 1027−1034.
(5) Posthuma-Trumpie, G. A.; Korf, J.; van Amerongen, A. Lateral flow (immuno)assay: its strengths, weaknesses, opportunities and threats. A literature survey. *Anal. Bioanal. Chem.* **2009**, *393*, 569−582.
(6) Sajid, M.; Kawde, A.-N.; Daud, M. Designs, formats and applications of lateral flow assay: A literature review. *J. Saudi Chem. Soc.* **2015**, *19*, 689−705.
(7) Bahadır, E. B.; Sezgintürk, M. K. Lateral flow assays: Principles, designs and labels. *TrAC, Trends Anal. Chem.* **2016**, *82*, 286−306.
(8) Dzantiev, B. B.; Byzova, N. A.; Urusov, A. E.; Zherdev, A. V. Immunochromatographic methods in food analysis. *TrAC, Trends Anal. Chem.* **2014**, *55*, 81−93.
(9) Fu, X.; Cheng, Z.; Yu, J.; Choo, P.; Chen, L.; Choo, J. A SERS-based lateral flow assay biosensor for highly sensitive detection of HIV-1 DNA. *Biosens. Bioelectron.* **2016**, *78*, 530−537.
(10) Cottat, M.; Thioune, N.; Gabudean, A.-M.; Lidgi-Guigui, N.; Focsan, M.; Astilean, S.; Lamy de la Chapelle, M. Localized Surface Plasmon Resonance (LSPR) Biosensor for the Protein Detection. *Plasmonics* **2013**, *8*, 699−704.
(11) Soler, M.; Huertas, C. S.; Lechuga, L. M. Label-free plasmonic biosensors for point-of-care diagnostics: a review. *Expert Rev. Mol. Diagn.* **2019**, *19*, 71−81.
(12) Romeo, A.; Leung, T. S.; Sanchez, S. Smart biosensors for multiplexed and fully integrated point-of-care diagnostics. *Lab Chip* **2016**, *16*, 1957−1961.
(13) Wang, Y.; Zhou, J.; Li, J. Construction of Plasmonic Nano-Biosensor-Based Devices for Point-of-Care Testing. *Small Methods* **2017**, *1*, No. 1700197.
(14) Abbas, A.; Tian, L.; Morrissey, J. J.; Kharasch, E. D.; Singamaneni, S. Hot Spot-Localized Artificial Antibodies for Label-Free Plasmonic Biosensing. *Adv. Funct. Mater.* **2013**, *23*, 1789−1797.
(15) Tian, L.; Morrissey, J. J.; Kattumenu, R.; Gandra, N.; Kharasch, E. D.; Singamaneni, S. Bioplasmonic Paper as a Platform for Detection of Kidney Cancer Biomarkers. *Anal. Chem.* **2012**, *84*, 9928−9934.
(16) Tian, L.; Liu, K.-K.; Morrissey, J. J.; Gandra, N.; Kharasch, E. D.; Singamaneni, S. Gold nanocages with built-in artificial antibodies for label-free plasmonic biosensing. *J. Mater. Chem. B* **2014**, *2*, 167−170.
(17) Tian, L.; Tadepalli, S.; Park, S. H.; Liu, K. K.; Morrissey, J. J.; Kharasch, E. D.; Naik, R. R.; Singamaneni, S. Bioplasmonic calligraphy for multiplexed label-free biodetection. *Biosens. Bioelectron.* **2014**, *59*, 208−215.
(18) Yin, Z.; Guo, H.; Li, Y.; Chiu, J.; Tian, L. Ultrastable Plasmonic Bioink for Printable Point-Of-Care Biosensors. *ACS Appl. Mater. Interfaces* **2020**, *12*, 35977−35985.
(19) Wang, C.; Wang, L.; Tadepalli, S.; Morrissey, J. J.; Kharasch, E. D.; Naik, R. R.; Singamaneni, S. Ultrarobust Biochips with Metal-Organic Framework Coating for Point-of-Care Diagnosis. *ACS Sens.* **2018**, *3*, 342−351.
(20) Li, Y.; Guo, H.; Yin, Z.; Lyle, K.; Tian, L. Metal−Organic Frameworks for Preserving the Functionality of Plasmonic Nanosensors. *ACS Appl. Mater. Interfaces* **2021**, *13*, 5564−5573.
(21) Tadepalli, S.; Yim, J.; Cao, S.; Wang, Z.; Naik, R. R.; Singamaneni, S. Metal-Organic Framework Encapsulation for the Preservation and Photothermal Enhancement of Enzyme Activity. *Small* **2018**, *14*, No. 1700197.
(22) Gupta, R.; Luan, J.; Chakrabartty, S.; Scheller, E. L.; Morrissey, J.; Singamaneni, S. Refreshable Nanobiosensor Based on Organosilica Encapsulation of Biorecognition Elements. *ACS Appl. Mater. Interfaces* **2020**, *12*, 5420−5428.
(23) Yetisen, A. K.; Akram, M. S.; Lowe, C. R. Paper-based microfluidic point-of-care diagnostic devices. *Lab Chip* **2013**, *13*, 2210−2251.
(24) Yang, Y.; Noviana, E.; Nguyen, M. P.; Geiss, B. J.; Dandy, D. S.; Henry, C. S. Paper-Based Microfluidic Devices: Emerging Themes and Applications. *Anal. Chem.* **2017**, *89*, 71−91.
(25) Akyazi, T.; Basabe-Desmonts, L.; Benito-Lopez, F. Review on microfluidic paper-based analytical devices towards commercialisation. *Anal. Chim. Acta* **2018**, *1001*, 1−17.
(26) Carrilho, E.; Martinez, A. W.; Whitesides, G. M. Understanding Wax Printing: A Simple Micropatterning Process for Paper-Based Microfluidics. *Anal. Chem.* **2009**, *81*, 7091−7095.
(27) Hong, W.; Zhou, J.; Kanungo, M.; Jia, N.; Dinsmore, A. D. Wax Spreading in Paper under Controlled Pressure and Temperature. *Langmuir* **2018**, *34*, 432−441.
(28) Altundemir, S.; Uguz, A. K.; Ulgen, K. A review on wax printed microfluidic paper-based devices for international health. *Biomicrofluidics* **2017**, *11*, 041501.
(29) Bruzewicz, D. A.; Reches, M.; Whitesides, G. M. Low-Cost Printing of Poly(dimethylsiloxane) Barriers To Define Microchannels in Paper. *Anal. Chem.* **2008**, *80*, 3387−3392.
(30) Dornelas, K. L.; Dossi, N.; Piccin, E. A simple method for patterning poly(dimethylsiloxane) barriers in paper using contact-printing with low-cost rubber stamps. *Anal. Chim. Acta* **2015**, *858*, 82−90.
(31) Jenkins, G.; Wang, Y.; Xie, Y. L.; Wu, Q.; Huang, W.; Wang, L.; Yang, X. Printed electronics integrated with paper-based microfluidics: new methodologies for next-generation health care. *Microfluid. Nanofluid.* **2015**, *19*, 251−261.
(32) Snyder, L. R.; Kirkland, J. J.; Dolan, J. W. Introduction. *Introduction to Modern Liquid Chromatography*, John Wiley & Sons, Inc.2009; pp 1−17.
(33) Riekkola, M.-L. Recent advances in nonaqueous capillary electrophoresis. *Electrophoresis* **2002**, *23*, 3865−3883.
(34) Aćimović, S. S.; Sipova, H.; Emilsson, G.; Dahlin, A. B.; Antosiewicz, T. J.; Kall, M. Superior LSPR substrates based on electromagnetic decoupling for on-a-chip high-throughput label-free biosensing. *Light Sci. Appl.* **2017**, *6*, No. e17042.
(35) Aćimović, S. S.; Ortega, M. A.; Sanz, V.; Berthelot, J.; Garcia-Cordero, J. L.; Renger, J.; Maerkl, S. J.; Kreuzer, M. P.; Quidant, R. LSPR chip for parallel, rapid, and sensitive detection of cancer markers in serum. *Nano Lett.* **2014**, *14*, 2636−2641.
(36) Chen, P.; Chung, M. T.; McHugh, W.; Nidetz, R.; Li, Y.; Fu, J.; Cornell, T. T.; Shanley, T. P.; Kurabayashi, K. Multiplex serum cytokine immunoassay using nanoplasmonic biosensor microarrays. *ACS Nano* **2015**, *9*, 4173−4181.
(37) Tian, L. M.; Chen, E.; Gandra, N.; Abbas, A.; Singamaneni, S. Gold Nanorods as Plasmonic Nanotransducers: Distance-Dependent Refractive Index Sensitivity. *Langmuir* **2012**, *28*, 17435−17442.
(38) Tian, L.; Fei, M.; Kattumenu, R.; Abbas, A.; Singamaneni, S. Gold nanorods as nanotransducers to monitor the growth and swelling of ultrathin polymer films. *Nanotechnology* **2012**, *23*, No. 255502.
(39) Joung, H. A.; Ballard, Z. S.; Ma, A.; Tseng, D. K.; Teshome, H.; Burakowski, S.; Garner, O. B.; Di Carlo, D.; Ozcan, A. Paper-based

https://doi.org/10.1021/acsami.1c24458
ACS Appl. Mater. Interfaces 2022, 14, 10729−10737

multiplexed vertical flow assay for point-of-care testing. *Lab Chip* **2019**, *19*, 1027−1034.
(40) Oh, Y. K.; Joung, H. A.; Kim, S.; Kim, M. G. Vertical flow immunoassay (VFA) biosensor for a rapid one-step immunoassay. *Lab Chip* **2013**, *13*, 768−772.
(41) Nikoobakht, B.; El-Sayed, M. A. Preparation and growth mechanism of gold nanorods (NRs) using seed-mediated growth method. *Chem. Mater.* **2003**, *15*, 1957−1962.
(42) Orendorff, C. J.; Murphy, C. J. Quantitation of metal content in the silver-assisted growth of gold nanorods. *J. Phys. Chem. B* **2006**, *110*, 3990−3994.

https://doi.org/10.1021/acsami.1c24458
ACS Appl. Mater. Interfaces 2022, 14, 10729−10737